1st Adiabatic Invariants and Phase Space Densities for the Jovian Electron and Proton Radiation Belts—Galileo and GIRE3 Estimates

H. B. Garrett[1] and I. Jun[1]

[1]The Jet Propulsion Laboratory, California Institute of Technology

Corresponding author: Insoo Jun (Insoo.Jun@jpl.nasa.gov)

Key Points:

- The long-term dynamics of particle trapping in the Jovian magnetosphere is investigated using high energy electron and proton data.
- 1st adiabatic invariant and phase space densities are computed using the EPD data as well as using the GIRE3 model.
- Both electrons and protons show a clear downward trend in flux and PSD at constant 1st adiabatic invariant as the planet is approached.

Abstract

The fluxes and phase space densities for a fixed 1st adiabatic invariant for high energy electrons and protons provide important inputs for various scientific studies for determining the physics of particle diffusion and energization. This study provides estimates of the 1st adiabatic invariant and phase space density based on the complete and large data base available from the Energetic Particle Detector (EPD) on Galileo for the jovian environment. To be specific, 10 minute averages of the high energy electron and proton data are used to compute differential flux spectra versus energy for L=~8 - 25 over the Galileo mission. These spectra provide estimates of the differential fluxes and phase space density for constant 1st adiabatic invariants between 10^2 to 10^5 MeV/G. As would be expected, the electron and proton fluxes and phase space densities generally trend lower as the planet is approached. The results indicate that, whereas the overall trends for each orbit are consistent, detailed orbit to orbit variations can be observed. Galileo orbit C22 is presented as a specific example of deviations from the mean downward trend. To validate the Galileo results and extend the findings into L=3, the GIRE3 model was also used to compute the fluxes and phase space densities for constant 1st adiabatic invariant versus L-shell. Comparison between GIRE3 and EPD demonstrates that the model adequately reproduces the EPD data trends and they consistently show additional variations near Io. This provides proof that the GIRE3 is a useful starting point for diffusion analyses and similar studies.

Plain Language Summary

Long term high-energy radiation environment at Jupiter is studied in this paper by using an extensive data set collected by the Galileo Energetic Particle Detector (EPD). This is the first time that the EPD high energy data are used in its entirety for this purpose. The results from the long-term (~7 years) observation confirm that trapped protons and electrons are indeed diffusing inward to the planet although there are some short-term orbit-to-orbit variations. This finding is shown to be consistent with the GIRE3 model output which has been and is being used for various Jovian mission designs (e.g., Juno, Europa Clipper, Europa Lander Concept Study)

1 Introduction

The last four decades have seen a significant increase in in-situ data on the jovian radiation belts. Following the Pioneer and Voyager flybys, Galileo observed the belts from 1995 through 2005 with 34 complete orbits. Recently, the Juno spacecraft has begun another long term mission to this king of planets. Unique to the various jovian missions, however, Galileo primarily orbited near Jupiter's equatorial plane with the bulk of its measurements at distances greater than ~8 Rj. Juno in contrast is primarily in a high inclination orbit with very low perijove flybys over the jovian poles—it will largely miss the radiation belts until late in its mission. Thus the Galileo data are of real value in mapping the equatorial radiation belts between 8 to 25 Rj—the region of particular interest to this study. To date, the Galileo data form an important data base for determining the physics of particle diffusion and energization in Jupiter's intense radiation belts (e.g., Nenon et al., 2018). Such studies are very dependent on the detailed variations of the fluxes and the phase space densities (PSD) at a constant 1st adiabatic invariant for high energy electrons and protons. To meet this need, the objective of this study is to provide estimates of the 1st adiabatic invariant fluxes and phase space densities based on the John

Hopkins Applied Physics Laboratory's (JHU/APL) Energetic Particle Detector (EPD) experiment (see Williams et al., 1992) on Galileo for high energy electrons in the range 0.1 MeV—100 MeV and protons between 0.6 MeV—100 MeV. (Note: The EPD data used here are from the "real time" collection mode and do include "record mode" collection mode data taken near the moons.)

To be specific, 10-minute averages of the EPD electron data channels are averaged to provide omni-directional differential fluxes at 0.238, 0.416, 0.706, 1.5, 2.0, 11.0, and 31 MeV (the latter energy based on Pioneer 10 and 11 measurements) and between 3.2-10.1 MeV for protons between L=~8 and L=25 for the 34 Galileo orbits. These allow determination of spectra which provide estimates for the differential fluxes and for the PSD for constant 1st adiabatic invariants between 10^2 MeV/G to 10^5 MeV/G along Jupiter's magnetic equator. The results permit studies of long term overall trends and orbit to orbit variations of these parameters. To illustrate the latter, the Galileo orbit C22 event is studied and provides valuable information on short period time variability.

An important additional tool in the analysis of the radiation environment at Jupiter is the GIRE family of plasma and high energy particle models (e.g., Divine and Garrett, 1983; Garrett et al. 2003, 2005, 2012, 2015, 2016; de Soria-Santacruz et al., 2016, 2017; Jun et al., 2019). The latest version of the GIRE3 model (Garrett et al., 2017; Jun et al., 2019) is an amalgam of synchrotron measurements and Pioneer, Voyager, and Galileo in-situ data. GIRE3 provides a definition of the electrons, protons, and various heavy ions between ~2 Rj and 50 Rj and for energies of a few eV to several 100 MeV/nucleon. Here GIRE3 will be used to compute the 1st adiabatic invariant and PSD versus L over the same range as the EPD data. GIRE3 also permits estimates of these key parameters into 3 Rj and of their variations near Io. Though the agreement between the EPD data and model is not unexpected as GIRE3 is based in part on the EPD data, it provides further proof that GIRE3 is a useful tool for diffusion analyses and similar studies and for evaluating the latest models of losses and sources in the critical inner radiation belts (see for example Woodfield et al., 2014).

This study is divided into two parts. First will be the computation of the 10 minute electron and proton fluxes and the PSD for fixed values of the 1st adiabatic invariant between ~8 and 25 L for the Galileo data. These were broken out by orbit to study temporal variations—an example of which, orbit C22, will be presented. In the second part we will carry out a similar analysis using the GIRE3 model between L=~3 and L=25. The electron and proton flux and phase space density contours versus energy are also computed to identify the applicable range of the analysis (i.e., between ~100 keV to 100 MeV for the electrons and ~600 keV to 100 MeV for the protons). Finally, the GIRE3 model and EPD variations with L will be compared and the results summarized.

2 Galileo Energetic Particle Detector (EPD)

The primary data source for this analysis is the Galileo APL/JHU EPD Low-Energy Magnetospheric Measurement System (LEMMS) which measures the high energy electrons and protons from Jupiter orbit insertion (JOI) in 1995 to the end of the mission in 2005 (Williams et al., 1992). Specifically, the steps undertaken to analyze Jupiter's trapped radiation in the jovian

magnetic equatorial plane in the range ~8 to ~25 Jupiter radii (1 jovian radius = 71,400 km) using the Galileo EPD data are described in this section. First, the 10-minute averages of the high-energy particle count rate data were combined with data on the location and magnetic field at the spacecraft—specifically, the position of the Galileo spacecraft and the magnetic field vector as modeled by the VIP4 magnetic field model (Connerney et al., 1998) from 8 to 25 L (L-shell, rather than R_J, was used in this study as the data are better ordered in terms of the magnetic field). Of the 32 LEMMS channels, the most important ones for radiation modeling are the electron channels B1 (1.5-10.5 MeV), DC2 ($\geq$2 MeV, and DC3 ($\geq$11 MeV) and the proton channel B0 (3.2-10.1 MeV). In addition, the F1 (174-304 keV), F2 (304-527 keV), and F3 (527-884 keV) channels were included for lower energy electrons. To provide an upper bound on the spectra at the highest energies, Pioneer 10 and 11 31 MeV measurements were added. Figure 1 is a plot of all the "raw" Planetary Data System (PDS) DC3 counts per second and the B0 differential fluxes to illustrate the variations of the EPD data with L-shell—over-plotted are the variations for Galileo orbit C22.

Consider first the electrons. The 7 EPD and 1 P10/11 electron channel count rates were converted to differential fluxes and fit with a spectrum of the form (Garrett et al., 2012):

$$J(E) = J_o E^{-A}\left(1 + {}^{E}/_{E_o}\right)^{-B} \quad (1)$$

where:

J = Isotropic differential electron flux as a function of E; $(cm^2\text{-s-sr-MeV})^{-1}$
E = Electron energy; MeV
J_0= Constant; $(cm^2\text{-s-sr-MeV})^{-1}$
A = Constant (approximately the power law index for the low-energy component)
B = Constant (A+B is approximately the power law index for the high-energy component)
E_0= Constant (approximately the breakpoint energy between low- and high-energy spectra); MeV

The constants J_0, A, B, and E_0 were computed for each 10 minute interval using EPD and Pioneer data from the PDS. As will be discussed below, the Eq. 1 constants then define a flux spectrum at each position that yields the electron 1st adiabatic invariant fluxes and the PSD functions.

Whereas computing the high energy electron flux spectra for the EPD data as just described was straightforward, computing the proton flux spectra was more involved. The primary reason is that the high energy electrons inwards of 25 Rj were found to contaminate the high energy EPD proton channels except for the B0 3.2-10.1 MeV channel (Jun et al, 2002). A proton flux spectrum in energy between 600 keV to 100 MeV is required to compute the fluxes and power spectral density for a specified 1st adiabatic invariant at a given point. Our method to do this assumes an appropriate proton spectrum scaled by the measured B0 flux at the point to the energy desired. Fortunately, APL has provided reference proton and heavy ion differential intensity spectra [Mauk et al., 2004] at 13 locations along the Galileo trajectory. These differential spectra, interpolated in L, are assumed to represent the shape of the proton flux distribution along the magnetic equator (Garrett et al., 2015). All the EPD ion data channels

between ~50 keV to ~50 MeV were simultaneously fit by APL to differential intensity spectra of the form given in Eq. (2) (Mauk et al., 2004):

$$J(E)_{APL} = C\,\frac{E[E_1+kT(1+\gamma_1)]^{-1-\gamma_1}}{1+(E_1/et)^{\gamma_2}} \qquad (2)$$

where:

C, *et*, *kT*, γ_1, γ_2 = Parameters for the APL spectral fits to the EPD data at 13 locations (Mauk et al., 2004; Eq. (1))

E_1 = Energy in reference frame of moving plasma (assumed = *E* in this study)

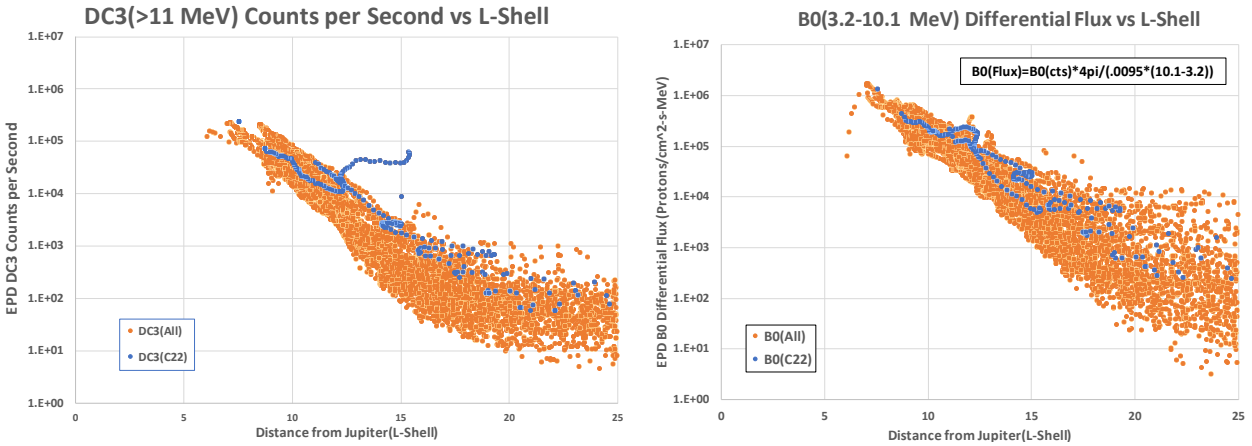

A) B)

Fig. 1. 10 minute averages of EPD observations for A) the DC3 electron channel counts and B) the B0 proton differential flux channel versus L-shell distance from Jupiter for all 34 orbits in orange. Also shown is orbit C22 (blue).

As described in Garrett et al. (2015), the selected APL proton spectra were interpolated in L between ~8—25 L. The resulting spectra were then scaled by the observed B0 flux at the desired point as derived from the PDS data. The estimated B0 fluxes (i.e., $J(B0)_{PDS}$) are plotted in Figure 1 and were computed as follows:

$$J(B0)_{PDS} = \frac{B0(Cts)\cdot 4\pi}{GF\cdot(10.1\ MeV - 3.2\ MeV)} \qquad (3)$$

where:

$J(B0)_{PDS}$ = B0 channel isotropic differential proton flux based on observed count rates; $(cm^2\text{-s-MeV})^{-1}$

B0(cts) = 10-minute averages of the B0 channel available from the PDS; (counts per second)

GF = Average Geometric Factor for B0 Channel; ~0.0094 cm^2-sr between 3.2–10.1 MeV (Jun et al., 2002)

To scale the proton distribution at an arbitrary energy at a given B0 data location, the GIRE3 model was exploited. As the GIRE3 proton model is based on the APL spectra (Garrett et al., 2015), the spectra given by Eq. (2) as interpolated in L are readily recovered at a given

location. That is, the GIRE3 differential flux at the desired energy/location was divided by the corresponding GIRE3 B0 flux at 5.69 MeV (the geometric mean of the B0 channel 3.2 to 10.1 MeV). The result, the normalized flux versus energy at the B0 data location, was then multiplied by the observed B0 flux value to give the corresponding flux at the desired energy. The formula is:

$$J(E)'_{PDS} = J(E)_G \frac{J(5.69)_{PDS}}{J(5.69)_G} \quad (4)$$

where:

$J(E)'_{PDS}$ = Estimated isotropic differential proton flux at given location and energy E; $(cm^2\text{-s-MeV})^{-1}$

$J(5.69)_{PDS}$ = Galileo PDS B0 flux at point

$J(E)_G$ = GIRE3 model flux at the required energy E and location

$J(5.69)_G$ = GIRE3 model flux at 5.69 MeV (the geometric mean of the B0 channel) and at the desired location

The requirement to be able to determine the electron and proton spectra at a given location for a specific energy follows from the methods used to determine the 1st adiabatic invariant and power spectral density. The 1st adiabatic invariant I in terms of the relativistic momentum, P, and the magnetic field, B, is given by (e.g., Roederer, 1970; McIlwain and Fillius, 1975):

$$I(\alpha) = (P^2 \sin^2\alpha)/2\, m_o B \quad (5)$$

The relativistic momentum can be shown to be given in terms of the particle kinetic energy E by:

$$P(E)c = (E^2 + 2EE_o)^{1/2} \quad (6)$$

where:

$I(\alpha)$ = 1st adiabatic invariant as a function of pitch angle, α; MeV/G

P = relativistic momentum; note: (Pc) is in units of MeV

E_o = rest mass energy; 0.511 MeV (electrons), 938 MeV (protons)

B = magnetic field strength; G

c = speed of light (multiplying P by c converts it to MeV)

m_o = mass of electron or proton

Assuming that the Galileo data are close to the magnetic equator and nearly isotropic (Garrett et al., 2012, 2015), α is 90°, and B_{eq} is the magnetic field at the equator, $I \sim P_\perp^2/2\, m_o B_{eq}$. Deviations from this approximation for Galileo are expected to be on the order of a factor of 2 or less as a result (McIlwain and Fillius, 1975). Eqs. 5 and 6 can then be inverted to give:

$$E = -E_0 + E_o\left[1 + 2B_{eq}I/E_o\right]^{1/2} \quad (7)$$

The procedure is to first define a value for I (e.g., 10^2 MeV/G,…10^5 MeV/G) for the electrons or protons. Eq. 7 then gives E for I and B_{eq} where B_{eq} is a function of L-shell and is given for each EPD data point. The differential flux for the electrons or protons at L is next computed for the value of E for the corresponding I and B_{eq}. L-shell and B_{eq} are computed using the VIP4 magnetic field model (Connerney et al., 1998). Results are plotted in Figures 2 and 3 for electrons and protons respectively for all Galileo orbits (note: the EPD data are plotted as dots, the solid and dashed lines are for the GIRE3 model and will be discussed in the next section). For reference, vertical black lines at L=10 and 22 in Figures 2 and 3 indicate the uncertainty (assumed to be +/- one standard deviation of the mean of the log of the fluxes in a 2 L bin interval) in the first adiabatic invariant (see also Jun et al. (2005) for a statistical error analysis of the EPD high energy electron data). This uncertainty varies from a factor of x2 inside 12 L to a factor of x6 to x10 at 24 L.

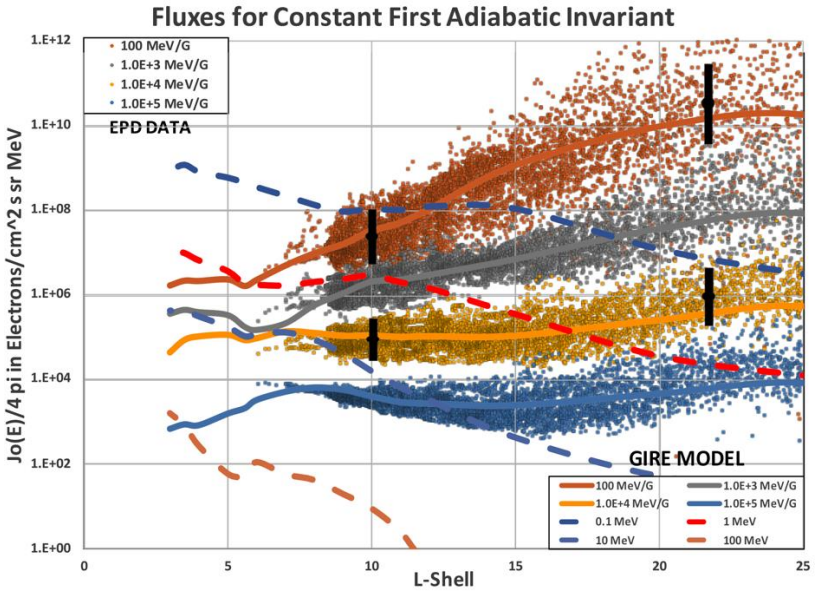

Fig. 2. Plot of 10 minute EPD electron fluxes for constant 1st adiabatic invariant I between 10^2 MeV/G to 10^5 MeV/G. Fluxes at constant I at similar values as determined by the GIRE3 model (solid lines) are also plotted. For reference, GIRE3 flux contours for constant energies between 0.1 MeV and 100 MeV, the assumed range of validity of the electron EPD data, are also shown as dashed lines.

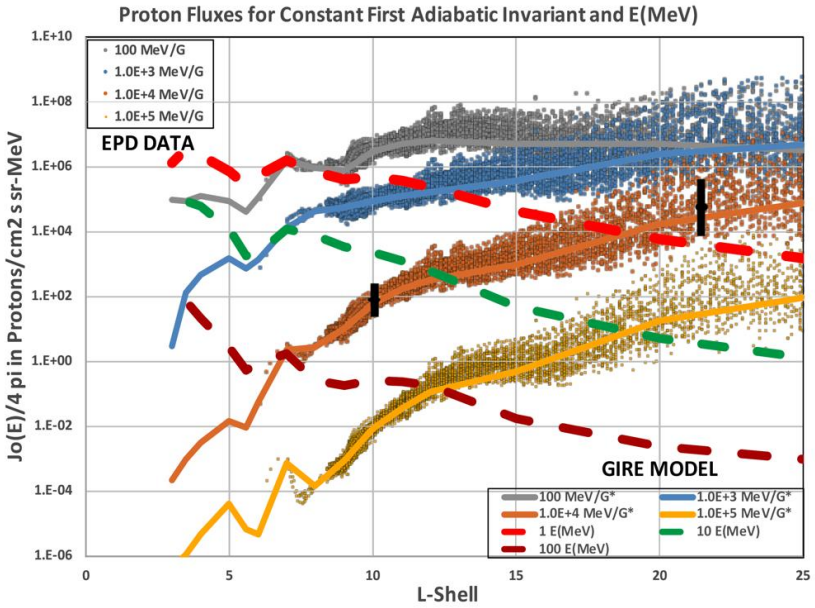

Fig. 3. Plot of 10 minute EPD proton fluxes for constant values of the 1st adiabatic invariant *I* between 10^2 MeV/G to 10^5 MeV/G. Also plotted are contours of constant *I* at similar values as determined by the GIRE3 model (solid lines). For reference, GIRE3 flux contours for constant energies between 1 MeV and 100 MeV are also shown as dashed lines (the EPD proton data are assumed to be valid between ~0.6 MeV and ~100 MeV).

The Galileo results are plotted for L values between L-shells of 8-25. The 25 L limit is imposed as a result of how the jovian plasma disc is modeled. While it is straightforward to compute values beyond ~25 L, the B_{eq} values in particular are very dependent on the magnetic field model assumed and L loses its relevance. Here the VIP4 model (Connerney et al., 1998) is assumed as opposed to the plasma sheet models of Khurana et al. (2005) which are used in the outer magnetosphere. The magnetic field models agree well inside 20 L but deviate significantly beyond ~25 L because of the complexities brought about by the jovian plasma disk.

The EPD data energy range of validity is also bounded as the flux contours for constant *I* indicate. That is, the EPD electron detectors are most reliable from ~170 keV (the EPD F1 channel lower energy) to ~30 MeV (the Pioneer 10 and 11). Even though the proton spectra provided by Mauk et al. (2004) were fit between ~50 keV to ~50 MeV, the validity of EPD low energy proton limit is estimated to be ~0.6 MeV (Garrett et al., 2015). At the high energy end, we have extrapolated both ranges up to 100 MeV, however, to allow for comparisons with the GIRE3 model inside L=10.

While the general trend of both the electrons and proton fluxes for the EPD constant 1st adiabatic invariants is towards lower values as the planet is approached, the electrons decrease by only 1 order of magnitude or less between 25 L and 8 L for 10^4 MeV/G to 10^5 MeV/G while the protons decrease by 2 orders of magnitude. Indeed, the EPD 10^4 MeV/G and 10^5 MeV/G electron 1st adiabatic constant fluxes are almost flat over this region and even rise slightly inside 10 L.

The second parameter of interest is the PSD. The PSD for relativistic particles is given explicitly (for constant 1st adiabatic constant *I*) by (e.g., Roederer, 1970; McIwain and Fillius, 1975):

$$F(I) = J'(I)/P'(I)^2 \quad (8)$$

where:

F = PSD as a function of constant I for either electrons of protons;
Note: F' is plotted in Figs. 4 and 5 where F' = F m^3 assuming that units of F' are s^3/km^6

J' = Isotropic differential flux as a function of E; $[cm^2\text{-s-sr-MeV}]^{-1}$

P' = Relativistic momentum, assumed to be $P_\perp^2$ here; $P_\perp$ is in units of MeV/c

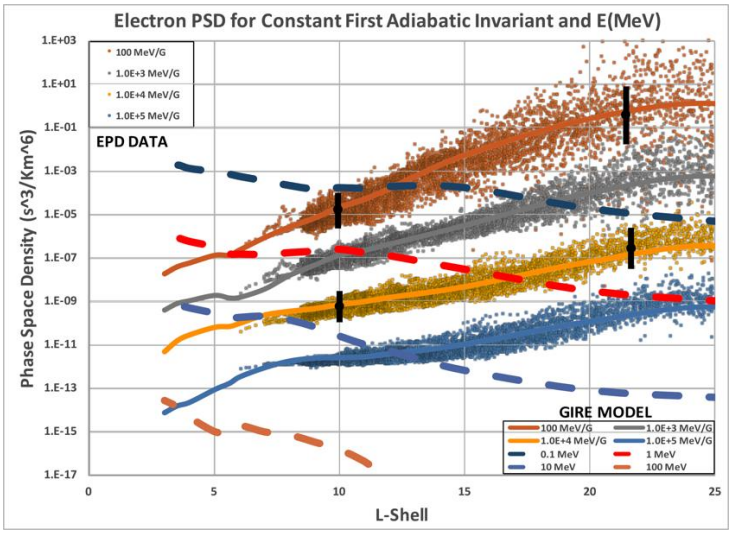

Fig. 4. Plot of 10 minute individual Galileo EPD electron PSDs for constant values of the 1st adiabatic invariant I between 10^2 MeV/G to 10^5 MeV/G. Additionally plotted are contours of constant PSD at similar values as determined by the GIRE3 model (solid lines). GIRE3 PSD contours for constant energies between 0.1 MeV and 100 MeV are also shown as dashed lines (see Fig. 2).

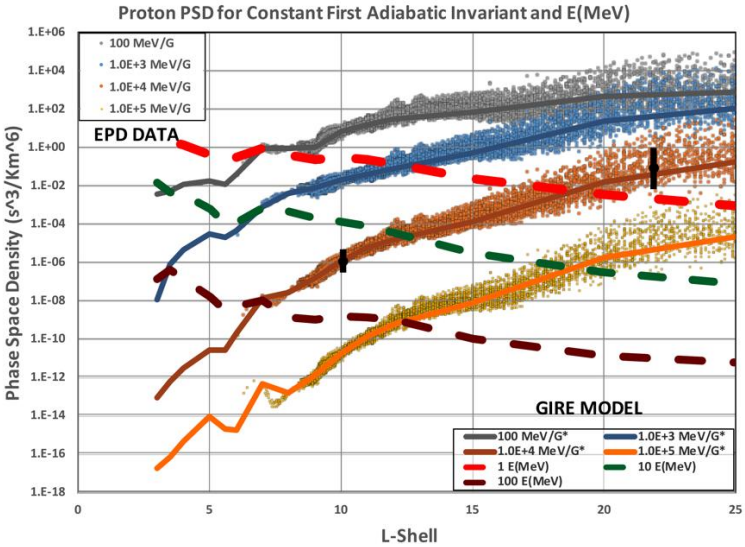

Fig. 5. Plot of 10 minute individual Galileo EPD proton PSDs for constant values of the 1st adiabatic invariant I between 10^2 MeV/G to 10^5 MeV/G. Additionally plotted are contours of constant PSD at similar values as determined by the GIRE3 model (solid lines). For reference, GIRE3 PSD contours for constant energies between 1 MeV and 100 MeV are also shown as dashed lines (see Fig. 3).

The PSD is very important for determining the sources and losses in the diffusion equation (Woodfield et al., 2014). For Jupiter, it is assumed that the main source of the trapped high energy particles is the inward diffusion and energization of lower energy particles (assumed to be the high energy tail of the plasma particles streaming outward in the equatorial plane) from outside ~25 Rj. The evidence for this inward diffusion in Figures 4 and 5 is the steady decrease of the PSD as one approaches the planet for both the electrons and protons. This has been reported by many authors for Jupiter such as McIlwain and Fillius (1975), Baker and Goertz (1976), Mogro-Campero and Fillius (1976), Thomsen et al. (1977), Cheng et al. (1983, 1985), and Woodfield et al. (2014). While the electron PSD falls off smoothly with L-shell, a slight flattening of the fall-off in the proton curves is visible where the PSD data have a small inflection between ~12 L and ~17 L (particularly in the 10^5 MeV/G contour). This is possibly associated with Ganymede near 15 L and, if the particles are infusing inward, may indicate it is a possible source of particles. There also appears to be a more rapid drop off at ~9 L that may represent absorption of inwardly diffusing particles by Europa. As for Figures 2 and 3, vertical black lines at L=10 and 22 in Figures 4 and 5 indicate the uncertainty (assumed to be +/- one standard deviation of the mean of the log of the fluxes in a 2 L bin interval) in the first adiabatic invariant. This uncertainty varies from a factor of x2 inside 12 L to a factor of x6 to x10 at 24 L.

The Galileo data can also be analyzed orbit by orbit. Although each of the orbits studied exhibit unique variations, orbit C22 (the 22nd orbit targeted for Callisto) is the most unusual as a major intensification of the high energy electrons was observed on Day 223 of 1999 as Galileo approached Jupiter. To illustrate the time evolution of the C22 observations, several of the EPD raw channels used in this study are plotted in Figure 6. The approximate duration of the C22 event is marked. Unfortunately, the EPD was not turned on sufficiently in advance to determine when the event actually started and it may have been in progress well before the data collection began. Also shown in Figure 6 are data from the Galileo Star Scanner which fill in the gaps in the EPD data (note: the Star Scanner also apparently did not record the beginning of the event). When available, the Star Scanner data typically parallel the DC3 count rates as it is apparently sensitive to high energy electrons (Fieseler et al., 2002). The Star Scanner data in Figure 6 imply that there were no other "unusual" impulses following the initial one. Finally, the periodic oscillations in the count rates are the results of the oscillations of the jovian magnetic field—plotting the data in terms of L-shell largely removes these variations.

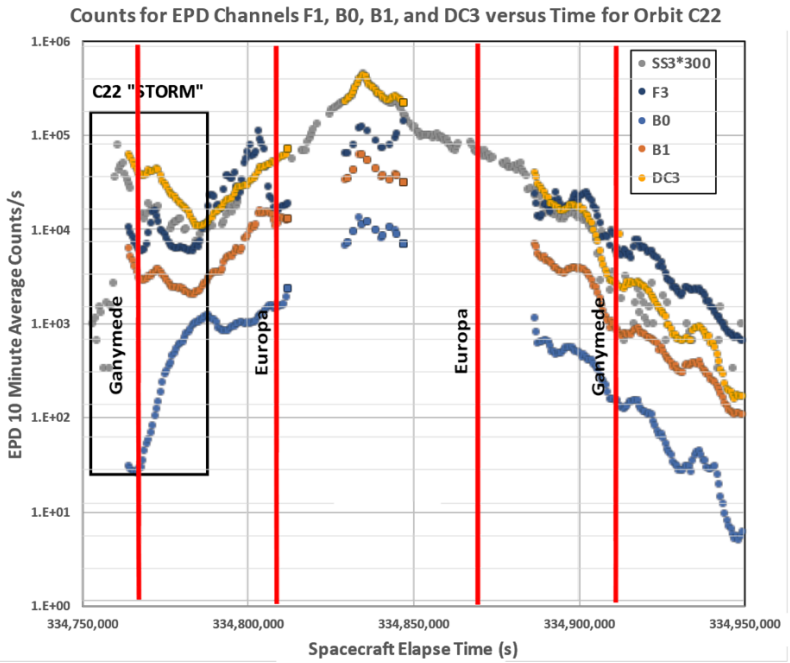

Fig. 6. Plot of 10 minute EPD counts per second for electron channels F3 (527-884 KeV), B1 (1.5-10.5 MeV), and DC3 (E≥11 MeV) and for proton channel B0 (3.2-10.1 MeV) for Galileo orbit C22. Also shown are the count rates for the Galileo Star Scanner (SS3) for the same time period scaled by x300. Time is shown as spacecraft elapsed time in seconds. The C22 "storm" interval is indicated by a box on the left. The times at which Galileo passed through the orbits of Europa and Ganymede are indicated but do not necessarily mean it flew by them.

Figure 7 plots the proton and electron fluxes and PSDs as functions of L-shell. The data are also divided into inward and outward portions of the C22 orbit (closed markers for inward and open markers for outward). While the protons show a bump at around 12 L, they basically follow the same trends in L as Figures 3 and 5. The electrons, however, show enhancements between 9-10 L near Europa and near L=15 (corresponding to the initial C22 impulse observation) for both the fluxes and PSDs (though 9-10 L impulse is much lower for the PSDs). These features are unique to the C22 orbit electrons. The enhancement between 9-10 L might indicate a source at Europa's orbit or perhaps an outwardly propagating enhancement near Io that is being shadowed by Europa—there is insufficient data inside 9 L to decide.

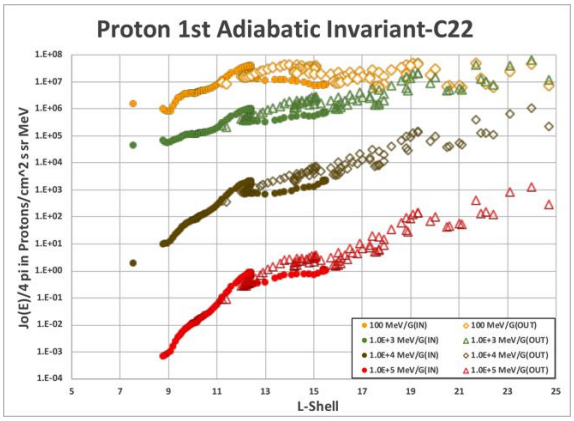

A.

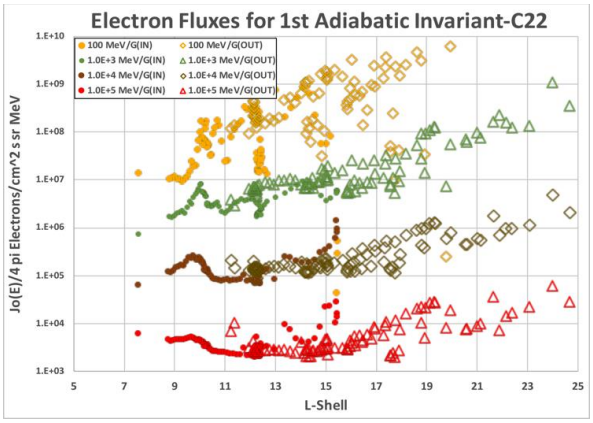

B.

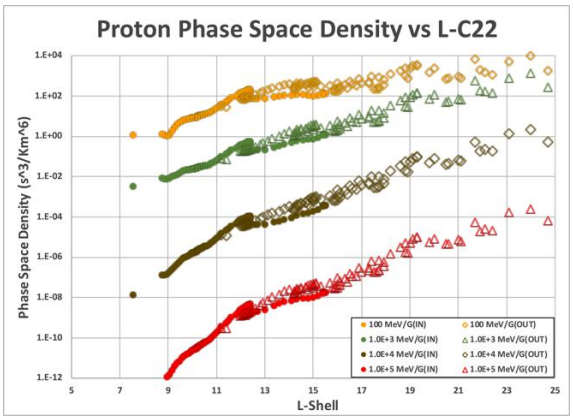

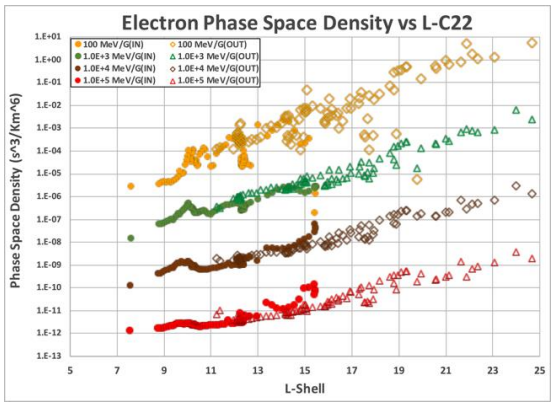

C. D.

Fig. 7. Plots of the 10 minute averages of the particle fluxes and PSD versus L-shell for the Galileo C22 orbit corresponding to Fig. 6. A) is a plot of the proton fluxes for constant 1st adiabatic invariants; B) is a plot of the electron fluxes for constant 1st adiabatic invariants; C) is a plot of the proton PSD for constant values of 1st adiabatic invariant; D) is a plot of the electron PSD for constant 1st adiabatic invariant.

3 GIRE3 Model Results

In this section, the GIRE3 model will be exploited to evaluate the electron and proton fluxes and phase space densities for constant 1st adiabatic invariant with the intent of comparing the model and EPD results. The GIRE family of jovian models has been used for some time (Divine and Garrett, 1983; Garrett et al. 2003, 2005, 2012, 2015, 2016; de Soria-Santacruz et al., 2016, 2017; Jun et al., 2019) to evaluate the radiation environment at Jupiter. As mentioned, the GIRE3 model is an amalgam of synchrotron measurements and Pioneer, Voyager, and Galileo in-situ data. The full model provides a definition of the electrons, protons, and various heavy ions between ~2 Rj and 50 Rj and for energies from a few eV to several 100 MeV/nucleon. Here the model is used to compute differential fluxes between 0.1 MeV and 100 MeV for the electrons and 0.6 MeV and 100 MeV for protons at selected energies versus L. The results in terms of constant 1st adiabatic invariant are converted to fluxes and PSDs for comparison with the EPD results. These are plotted as overlays in Figures 2, 3, 4, and 5 as solid lines. As would be anticipated since the GIRE3 model is based in part on the EPD data, there is agreement between 8 L and 25 L—the model appears to trace the mean of the EPD 10 minute electron and proton constant 1st adiabatic invariants. The comparisons provide proof that GIRE3 is a useful reference for diffusion analyses and for evaluating the latest models of losses and sources in the critical inner radiation belts.

To investigate the role of the jovian moons Io and Europa on the 1st adiabatic invariant flux and the PSD as modeled by GIRE3, the GIRE3 model was run into 3 L. The results are shown as overlays in Figs. 2, 3, 4, and 5 as solid lines. While for electrons the 10^2, 10^3, and 10^4 MeV/G 1st adiabatic invariant fluxes appear to show structure near L-shells associated with Io (5-6 L) in Figure 2, there is minimal evidence for it in the 10^5 MeV/G (Figure 2) and the PSD plots (Figure 4). Indeed the GIRE3 contour plots imply that the PSDs drop off fairly smoothly inside the orbit of Europa into L=3. In contrast the protons show definite structure inside L=8. Both in Figures 3 and 5, there appears to be an initial increase around 7 L followed by a drop into 5-6 L followed by another increase and then a fall off inside Io's orbit. Io may be acting as a block for the inward diffusing protons. These latter variations may be suspect for portions of the 10^4 and

10^5 MeV/G 1st adiabatic invariant proton contours, however, as the GIRE3 predictions occur at energies above the 100 MeV proton energy contour (i.e., the dark red/purple dashed line which indicates the approximate upper energy bound of 100 MeV of the GIRE3 model).

4 Summary and Conclusion

The objective of this paper was to investigate the variations in the flux and PSD at constant 1st adiabatic invariant between L=~8 and L=25 in the jovian equatorial plane for the high energy electrons and ions over the Galileo mission using the JHU/APL EPD data. Thus, the results reported in this paper represents a general long-term trend of particle trapping in the jovian radiation belts. In addition, the results were compared with the GIRE3 jovian particle model. The latter allowed the analysis to be extended into L=~3. As illustrated in Figures 2, 3, 4, and 5, the general trend of the electron and proton fluxes and PSDs for a given 1st adiabatic invariant was to decrease from L=25 to L=3. This is generally assumed to indicate the inward diffusion and energization of the electrons and protons and is consistent with current observations and understanding of the sources of the jovian radiation belts. A new finding in this study is the more rapid fall off (factor of 100) in the fluxes or the PSDs of the protons with L as compared to the electrons. While the electrons and protons show gradual changes in slope between Ganymede and Europa, the protons show much higher order variations between 10 L and 3 L (i.e., near the locations of Europa and Io).

The Galileo data set also allows the study of individual orbits. One example, the iconic C22 orbit presented here, shows detail in the 1st adiabatic invariant contours that is not visible in the overall mission set and in the GIRE3 predictions. As discussed, the proton fluxes and PSDs show little evidence of the initial impulse and, as the planet is approached, appear to be depressed although there is a peak at about L=12. The electrons, on the other hand, clearly show the impulsive event at L=15 which drops off rapidly as the planet is approached followed by another impulse at the orbit of Europa.

To conclude, the Galileo EPD high energy electron and proton data and the GIRE3 Jupiter environmental model both provide useful and consistent information on the variations of the jovian fluxes and PSDs for constant 1st adiabatic invariants. While both electrons and protons show a clear downward trend in flux and PSD at constant 1st adiabatic invariant as the planet is approached, the protons appear to fall off much more rapidly. This may indicate that the high energy protons are not diffusing inwards as fast as the electrons. While the GIRE3 model predictions provide "mean" predictions of the electrons and protons from L=25 well into L=3, the Galileo data permit the study of orbit by orbit variations as exemplified by orbit C22. Finally, the Galileo data and the GIRE3 model potentially provide valuable inputs for studies of inward particle diffusion and energization at Jupiter.

Acknowledgements

The research described in this paper was carried out at the Jet Propulsion Laboratory, California Institute of Technology, under a contract with the NASA (80NM0018D0004). The primary source and inspiration for this work was the authors' friend and mentor, T. Neil Divine, who developed the initial programs and processes on which the GIRE model is based. The updates

would not have been possible without the significant contributions by personnel at JPL (R. W. Evans and J. M. Ratliff) and at the Johns Hopkins University Applied Physics Laboratory (e.g., R. McEntire, D. Williams, C. Paranicas, and B. Mauk) who provided the energetic-particle-detector data from Galileo. The authors also thank J. E. P. Connerney and K. K. Khurana for allowing the use of their magnetic-field models. Finally, the authors owe special thanks to the Planetary Data System (S. Joy and others) who assisted in securing much of the data used here. Data used in this paper to create the figures will be uploaded to https://data.nasa.gov when the paper is accepted for publication.

References

Baker, D. N., and C. K. Goertz (1976), Radial diffusion in Jupiter's magnetosphere, *J. Geophys. Res.*, 81 (28), pp. 5215-5219.

Cheng, A. F., C. G. Maclennan, L. J. Lanzerotti, M. T. Paonessa, and T. P. Armstrong (1983), Energetic ion losses near Io's orbit, *J. Geophys. Res.*, 88 (A5), pp. 3936-3944.

Cheng, A. F., S. M. Krimigis, and T. P. Armstrong (1985), Near equality of ion phase space densities at Earth, Jupiter, and Saturn, *J. Geophys, Res.*, 90 (A1), pp. 526-530

Connerney, J.E., M.H. Acuna, N.F. Ness, and T. Satoh (1998), New models of Jupiter's magnetic field constrained by the Io flux tube footprint, *J. Geophys. Res.*, 103 (A6), 11929–11940, 1998.

de Soria-Santacruz, M., Garrett, H. B., Evans, R. W., Jun, I., Kim, W., Paranicas, C., and Drozdov, A. (2016), An empirical model of the high-energy electron environment at Jupiter, *J. Geophys. Res.*, pp. 1-12, 2016. doi: 10.1002/2016JA023059.

de Soria-Santacruz, M., Y. Y. Shprits, A. Drozdov, J. D. Menietti, H. B. Garrett, H. Zhu, A. C. Kellerman, and R. B. Horne (2017), Interactions between energetic electrons and realistic whistler mode waves in the Jovian magnetosphere, *J. Geophys. Res.*, 122, doi:10.1002/2017JA023975.

Divine, N. T., and H. B. Garrett (1983), Charged Particle Distributions in Jupiter's Magnetosphere, *J. Geophys. Res.*, 88, 6889-6903.

Fieseler, P. D., S. M. Ardalan, and A. R. Frederickson (2002), The Radiation Effects on Galileo Spacecraft Systems at Jupiter, *IEEE Trans. Nuc. Sci.*, Vol. 49, No. 6.

Garrett, H. B., I. Jun, J. M. Ratliff, R. W. Evans, G. A. Clough, and R.W. McEntire (2003), Galileo Interim Radiation Electron Model, *JPL Publication 03-006*, 72 pages, The Jet Propulsion Laboratory, California Institute of Technology, Pasadena, CA.

Garrett, H. B., S. M. Levin, S. J. Bolton, R. W. Evans, B. Bhattacharya (2005), A revised model of Jupiter's inner electron belts: Updating the Divine radiation model, *Geophys. Res. Lett.*, Vol. 32, No. 4, L04104 http://dx.doi.org/10.1029/2004GL021986.

Garrett, H. B., M. Kokorowski, I. Jun, and R. W. Evans (2012), Galileo Interim Radiation Electron Model Update—2012, *JPL Publication 12-9*. https://trs.jpl.nasa.gov/handle/2014/42026.

Garrett, H. B., Martinez-Sierra, Luz Maria, and Evans, R. W. (2015), Updating the Jovian Proton Radiation Environment—2015, *JPL Publication 15-9*, pp. 36, http://hdl.handle.net/2014/45463.

Garrett, H. B., W. Kim, and R. W. Evans, (2016), Updating the Jovian Plasma and Radiation Environments: The Latest Results for 2015, *Journal of Spacecraft and Rockets*, pp. 1-15. doi: 10.2514/1.A33510

Garrett, H. B., I. Jun, R. W. Evans, W. Kim, and D. Brinza, (2017), The Latest Jovian-Trapped Proton and Heavy Ion Models", *IEEE Trans. Nuc. Sci.*, Vol. 64, Issue 11, pp. 2802–2813, doi 10.1109/TNS.2017.2755618.

Jun, I., J. M. Ratliff, H. B. Garrett, and R. W. McEntire (2002), Monte Carlo simulations of the Galileo Energetic Particle Detector, *Nuc. Instr. and Methods in Phys. Res*., A, Vol. 490, 465-475.

Jun, I., H. B. Garrett, R. Swimm, R. W. Evans, and G. Clough (2005), Statistics of the variations of the high-energy electron population between 7 and 28 jovian radii as measured by the Galileo spacecraft, *Icarus*, Vol. 178, pp. 386-394, doi:10.1016/j.icarus.2005.01.022.

Jun, I., H. B. Garrett, and R. W. Evans (2019), Trapped Electron Environments of the Outer Planets, *IEEE Trans. Plasma Sci.*, Vol. 47, No. 8, pp, 3923-3930, doi: 10.1109/TPS.2019.2907069 .

Khurana, K. K., and H. K. Schwarzl (2005), Global structure of Jupiter's magnetospheric current sheet, J. Geophys. Res., 110 (A07227). doi:10.1029/2004JA010757.

Mauk, B. H., D. G. Mitchell, R. W. McEntire, C. P. Paranicas, E. C. Roelof, D. J. Williams, S. M. Krimigis, and A. Lagg (2004), Energetic ion characteristics and neutral gas interactions in Jupiter's magnetosphere, *J. Geophys. Res., 109, A09S12, doi:10.1029/2003JA010270.*

McIlwain, C. E., and R. W. Fillius (1975), Differential Spectra and Phase Space Densities of Trapped Electrons at Jupiter, *J. Geophys. Res.*, Vol. 80, No. 10, pp. 1341-1345.

Mogro-Campero, A., and W. Fillius (1976), The absorption of trapped particles by the inner satellite of Jupiter and the radial diffusion coefficient of particle transport, *J. Geophys. Res.*, 81 (7), pp. 1289-1295.

Nenon, Q., A. Sicard, P. Kollman, H. B. Garrett, S. P. A. Sauer, and C. Paranicas (2018), A Physical Model of the Proton Radiation Belts of Jupiter Inside Europa's Orbit, *J. Geophys. Res.: Space Physics*, 123, 3512–3532, https://doi.org/10.1029/ 2018JA025216.

Roederer, J. G. (1970), Dynamics of geomagnetically trapped radiation", *Springer-Verlag*, New York, New York, 166 p.

Thomsen, M. F., C. K. Goertz, and J. A. Van Allen (1977), On determining magnetospheric diffusion coefficients from the observed effects of Jupiter's Satellite Io, *J. Geophys, Res.*, 82 (35), pp. 5541-5550.

Williams, D. J., R. W. McEntire, S. Jaskulek, and B. Wilken (1992), The Galileo Energetic Particle Detector, in *The Galileo Mission,* edited by C.T. Russell, pp. 385–412, Kluwer Academic Publishers, Dordrecht, The Netherlands.

Woodfield, E. E., R. B. Horne, S. A. Glauert, J. D. Menietti, and Y. Y. Shprits (2014), The origin of Jupiter's outer radiation belt, *J. Geophys. Res. Space Physics*, 119, pp. 3490–3502, 2014, doi:10.1002/2014JA019891.